Investigation of dominant spin wave modes by domain walls collision

M. Ramu, I. Purnama, S. Goolaup, M. Chandra Sekhar, and W. S. Lew

---

Articles you may be interested in

Propagating and reflecting of spin wave in permalloy nanostrip with 360° domain wall
J. Appl. Phys. **115**, 013908 (2014); 10.1063/1.4861154

Spin-wave resonance reflection and spin-wave induced domain wall displacement
J. Appl. Phys. **113**, 213904 (2013); 10.1063/1.4808298

Spin-wave excitations induced by spin current through a magnetic point contact with a confined domain wall
Appl. Phys. Lett. **101**, 092405 (2012); 10.1063/1.4745777

Effect of nonadiabatic spin transfer torque on domain wall resonance frequency and mass
Appl. Phys. Lett. **98**, 092501 (2011); 10.1063/1.3560305

Spin wave assisted current induced magnetic domain wall motion
Appl. Phys. Lett. **96**, 242501 (2010); 10.1063/1.3446833

Investigation of dominant spin wave modes by domain walls collision

M. Ramu, I. Purnama, S. Goolaup, M. Chandra Sekhar, and W. S. Lew[a]
School of Physical and Mathematical Sciences, Nanyang Technological University, 21 Nanyang Link, Singapore 637371

Spin wave emission due to field-driven domain wall (DW) collision has been investigated numerically and analytically in permalloy nanowires. The spin wave modes generated are diagonally symmetric with respect to the collision point. The non-propagating mode has the highest amplitude along the middle of the width. The frequency of this mode is strongly correlated to the nanowire geometrical dimensions and is independent of the strength of applied field within the range of 0.1 mT to 1 mT. For nanowire with film thickness below 5 nm, a second spin wave harmonic mode is observed. The decay coefficient of the spin wave power suggests that the DWs in a memory device should be at least 300 nm apart for them to be free of interference from the spin waves. © 2014 AIP Publishing LLC. [http://dx.doi.org/10.1063/1.4885453]

I. INTRODUCTION

The proposal of magnetic solid-state memory for non-volatile high-density storage devices has stimulated intensive research in magnetic domain wall (DW) dynamics.[1,2] In such devices, the data are stored by means of a controlled magnetization reversal over a specific region of a patterned nanowire.[3,4] As a result of the reversal process, multiple DWs are created along the nanowire to separate the data. Spin-polarized current is then applied to the nanowire (NW) to move the DWs (and consequently, the data) to the write/read sensor.[5–8] As the effectiveness of the spin-transfer torque from the current to the DW is highly dependent on the magnetization configuration of the nanowire, the noise within the device should be as low as possible. One possible source of signal noise that can be expected in the DW-based magnetic device is spin wave (SW). Micromagnetic simulations have shown that the dynamics of a DW within a nanowire can be affected by spin waves propagating at high speeds.[9,10] Such spin waves can be found within the nanowire in various situations.[11,12] For instance, it has been shown that spin waves are emitted when vortex and anti-vortex cores are annihilated.[13,14] As spin waves can travel over few micrometer (μm) and last for few nanosecond (ns), they can be detrimental to the memory device by disturbing the DW dynamics. Thus, it is important to understand the characteristics of those spin waves and how they are related to the device parameters.

In this work, we report on the property of spin waves generated from the collision of two transverse DWs in a magnetic nanowire. Such DW-DW collision phenomenon can happen when a magnetic data bit is being erased from the memory device. Our results show that spin wave modes generated on one side of the collision point are diagonally symmetric with respect to the collision point, with the non-propagating mode having the highest amplitude. The frequency of the fundamental mode is strongly correlated to

the geometrical parameters of the wire. For nanowire with film thickness less than 5 nm, the appearance of a second-harmonic mode is observed, due to the strong demagnetizing field perpendicular to the plane of the wire.

II. MICROMAGNETIC MODELING

The DW collision phenomenon[15,16] is investigated by using the OOMMF micromagnetic simulation software that is based on the Landau-Lifshitz-Gilbert (LLG) equation[17]

$$\frac{dM}{dt} = -\gamma(M \times H_{eff}) + \frac{\alpha\gamma}{M_s}\left\{M \times (M \times H_{eff})\right\}, \quad (1)$$

where M is the local magnetization vector, α is Gilbert damping constant, γ is the gyromagnetic ratio, and H_{eff} is the effective magnetic field. Shown in Fig. 1(a) is the schematic of the simulated structure: a rectangular nanowire which is 30 μm long and 100 nm wide with a thickness of 6 nm. The length of the nanowire is chosen so as to avoid spin wave reflections from the end points of the nanowire. The nanowire is discretized into cell size of $5 \times 5 \times 6$ nm^3, in the x, y, and z directions, respectively. The material parameters used in the simulations are for Ni$_{80}$Fe$_{20}$: saturation magnetization $M_s = 8.0 \times 10^5$ A/m, exchange stiffness constant $A = 1.3 \times 10^{-11}$ J/m, damping constant $\alpha = 0.01$, and zero magneto-crystalline anisotropy.

III. RESULTS AND DISCUSSIONS

Initially, a transverse head-to-head (HH) and tail-to-tail (TT) DWs are nucleated at a distance of -13 μm and $+13$ μm from the center of the nanowire, respectively. The two DWs have the same chirality, with transverse components pointing along $-y$ axis. An external in-plane magnetic field H_a is then applied along $+x$ direction. Driven by the external field, the HH and TT DWs move towards the center of the nanowire, where they collide and annihilate each other. The annihilation is possible because the two DWs have different edge defects.[18,19] Fig. 1(b) shows a snapshot of the spatial distribution of spin configuration within the

[a]Author to whom correspondence should be addressed. Electronic mail: wensiang@ntu.edu.sg
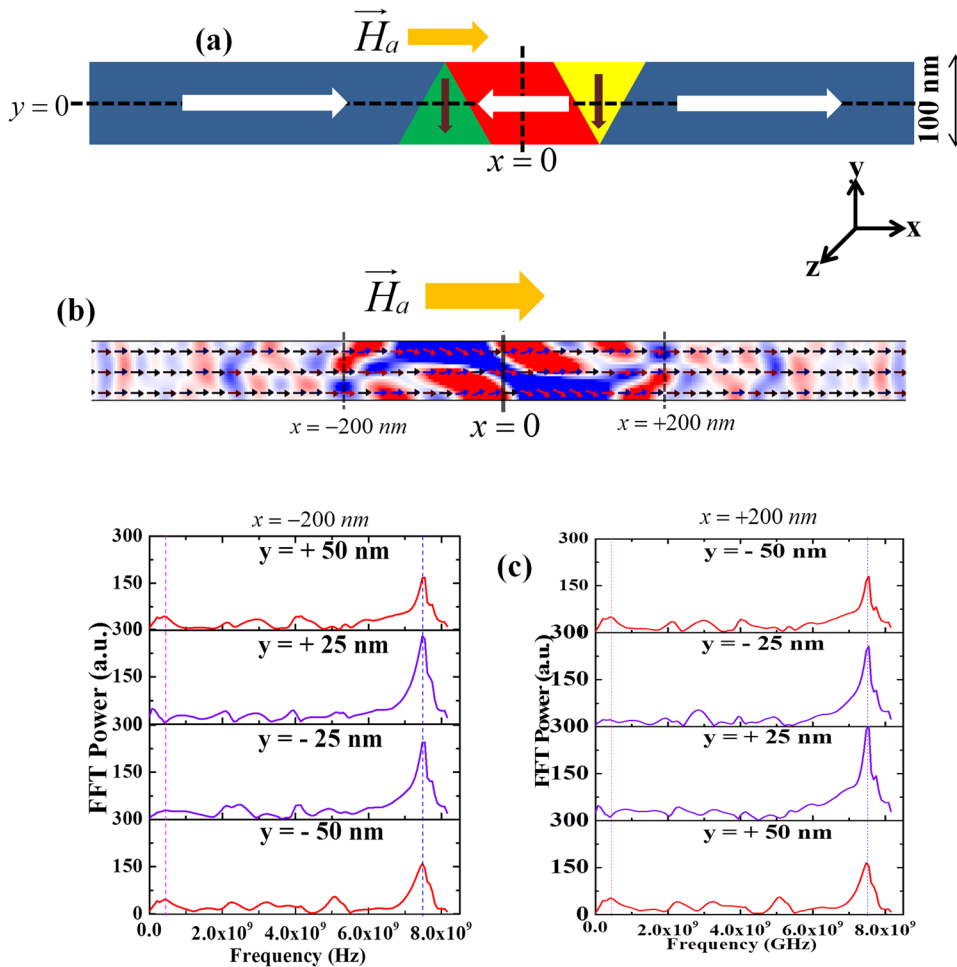
FIG. 1. (a) Schematic representation of the model employed in our micromagnetic simulations: A head-to-head (green color) and a tail-to-tail (yellow color) DWs are aligned in $-y$ axis. H_a is an external field applied along x-direction to drive the DWs. (b) Snapshot image of the spatial distribution of the magnetization profile at $t = 2$ ns after the collision. (c) SW spectra obtained from FFTs of $m_y(t)$ recorded at various positions along the width of the wire. These probe points are placed at a distance of $x = \pm 200$ nm away from the collision point (x = 0). The modes along the right vertical dashed line represent the fundamental modes, while the one along the left vertical dashed line represents the edge modes.

nanowire at 2 ns after the collision. The magnetic moments in the x-direction align along the wire length, except for a slight canting of spins close to the collision point. The dark color contrast close the collision point implies that there is a strong perturbance of the magnetization component along the y and z directions. The color contrast along the length of the nanowire indicates that SWs are emitted and are being propagated towards both ends of the nanowire. By comparing the spin configurations at various points in the space, it is clear that magnetization profiles on either side of the collision points are anti-symmetric.

To better understand this effect, probe points were placed along the width of the nanowire, on either side of the collision point ($x = 0$). At these probe points, we have recorded the temporal evolution of the magnetization. The total simulation time is about 60 ns. Spectra of SW modes are obtained from the temporal evolution of magnetization via 1D Fast Fourier Transformation (FFT).[11,20] A 2D matrix comprising the normal component of transverse magnetization (m_y) and simulation time (t) at these probe points is initially formed. Individual FFTs are then performed at every point along the line, for which the sampling rate is considered to be 60 ps. In Fig. 1(c), we present the SW spectra as a function of wire width for various probe points positioned at $x = \pm 200$ nm from the collision point. It can be clearly seen from Fig. 1(c) that the high frequency (7.5 GHz) fundamental mode with wave vector $(k) = 0$ exists uniformly along the

width. However, the amplitude of this mode is higher at the centre of the NW width ($y = 0$ nm) and decreases towards the edge of the wire. Besides the fundamental mode, low amplitude propagating modes can also be seen. At the wire edges ($y = +50$ nm and -50 nm), we note the appearance of additional modes. These edge modes[21] are due to the inhomogeneity in the profile of internal static magnetic field near the edges of the wire. Due to this, the precession frequency near the edges is different than in the central region. These modes are analogous to the Damon-Eschbach magnetostatic modes[22–24] appearing in continuous magnetic films. From Fig. 1(c), the additional edge modes along nanowire width show a diagonally symmetric behaviour with respect to the collision point. The modes at the edge of the nanowire, $x = (+)-200$ nm and $y = (-)+50$ nm, have the same profile of power spectra as at edge $x = (-)+200$ nm and $y = (+)-50$ nm.

From a device perspective, the low amplitude propagating mode will not significantly affect DW dynamics. As such, we focus solely on the fundamental mode produced by the DW collision. To obtain the decay characteristics of the fundamental spin waves mode, which arises due to the damping term in LLG equation, individual FFTs are computed at various probe points along $y = 0$ nm, where the mode has the highest amplitude. Shown in Fig. 2 are the amplitudes of the power spectra as a function of distance from the collision point. The inset of Fig. 2 shows the power spectra of the
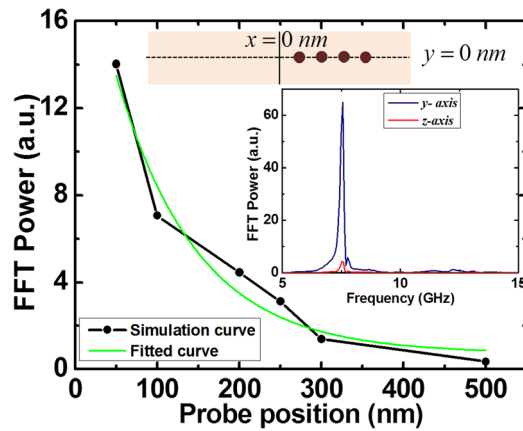
FIG. 2. (a) Power spectra of the spin waves measured at the probe points along the line $y = 0$. The applied field strength is 0.3 mT, the width of the nanowire is 100 nm, and the thickness is 6 nm. Inset shows power spectra corresponding to the transverse (m_y) and perpendicular (m_z) magnetization at $x = -200$ nm and $y = 0$ nm.

transverse (in-plane, along y-axis) and perpendicular (out-of-plane, along z-axis) SW modes obtained at $x = -200$ nm and $y = 0$ nm. Due to lateral confinement of the nanowire, SW modes are excited only along y and z-directions. For fixed field and geometrical parameters, SW modes along both orientations have similar frequency; however, the power of the transverse wave is found to be significantly higher than that of the perpendicular wave. Due to the shape anisotropy, a stronger demagnetizing field acts along the z axis of the nanowire. As such, we have only considered the effect of the transverse component of the magnetization in this work. As seen from Figure 2, the spin wave power drops exponentially as it travels along the length of the nanowire. The curve fitting gives us a decay coefficient of $\beta = 98$ nm. The curve shows that the spin wave power drops to around to 10% at a distance of 350 nm away from the collision point.

To gain an insight into the effect of geometrical parameters on the fundamental SW mode generated during collision, we have varied the wire width from 50 nm to 150 nm. The upper bound for the width is set by the stability of the transverse DW.[25] Shown in Figure 3(a) is the frequency of the fundamental mode (transverse component) as a function of wire width measured along the line $y = 0$ nm, at a distance of $x = 200$ nm from the collision point. The film thickness was kept at 6 nm. A clear red-shift is observed for the fundamental modes as the nanowire width is increased. The inset in Fig. 3(a) shows the FFT power spectra for SW mode perpendicular to the wire (z-axis). As can be seen, similar red shift is observed and the frequency of the fundamental modes is consistent with that obtained along the y-axis. Interestingly, we note that the peak for the 50 nm wide nanowire is more prominent along the z-axis. This is due to the fact that as the wire width reduces the demagnetization field along the width and perpendicular to the plane of the wire becomes comparable, thus the peaks have similar amplitude.

The obtained frequencies for the transverse component are plotted against the Kittel's equation,[26,27] which can be used to probe the spin dynamics of a ferromagnetic material
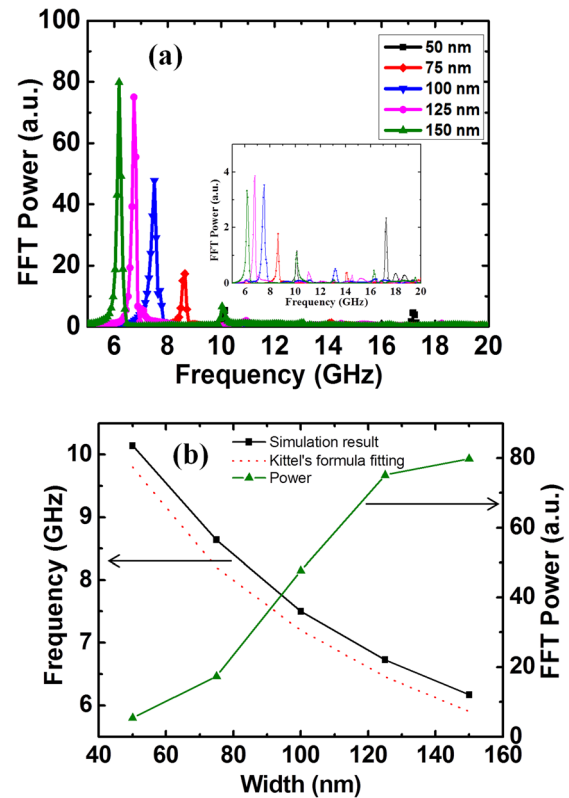
FIG. 3. (a) Power spectra of the spin waves for different widths of the nanowire. Inset figure shows power spectra of spin wave obtained from FFTs of $m_z(t)$. (b) The frequency and power of the fundamental modes as a function of the width of the nanowire.

$$f = \frac{\gamma}{2\pi}\sqrt{(H_{eff} + (N_z - N_x)M_s) \times (H_{eff} + (N_y - N_x)M_s)}, \quad (2)$$

$$N_x + N_y + N_z = 1, \quad (3)$$

where f is the frequency of the spin wave, N_x, N_y, and N_z are the demagnetization factors along the respective axes. For an infinitely long nanowire, the demagnetization factor along the x-axis becomes negligible ($N_x \sim 0$). The effective field is approximated by the applied field ($H_{eff} = H_a$). The Kittel's equation can then be modified as

$$f = \frac{\gamma}{2\pi}\sqrt{H_a^2 + M_s H_a + N_y(1 - N_y)M_s^2}. \quad (4)$$

Shown in Fig. 3(b) is the plot of the frequency of the fundamental mode as a function of the nanowire width. The obtained frequencies of the fundamental modes from the simulations are shown to match well with those obtained from the Kittel's equation, which is typically used to describe non-propagating spin waves. The DW collision can then be said to excite both the propagating and the non-propagating waves, with the non-propagating waves possessing the highest amplitude, which in turn may affect the dynamics of neighboring DWs.[10] The results also show that the decrease in the spin wave frequency for wider nanowire is accompanied by an increase in the FFT power, which can be understood as the result of the system trying to preserve the total energy of the generated spin waves.

Fig. 4(a) shows the FFT power spectra of the spin wave, measured at $x = 200$ nm and $y = 0$ nm, as the $Ni_{80}Fe_{20}$ film

FIG. 5. Power spectra of the fundamental mode for different applied field strengths at fixed NW dimensions. The frequency of the mode is found to be 7.6 GHz, which is constant for all field strengths.
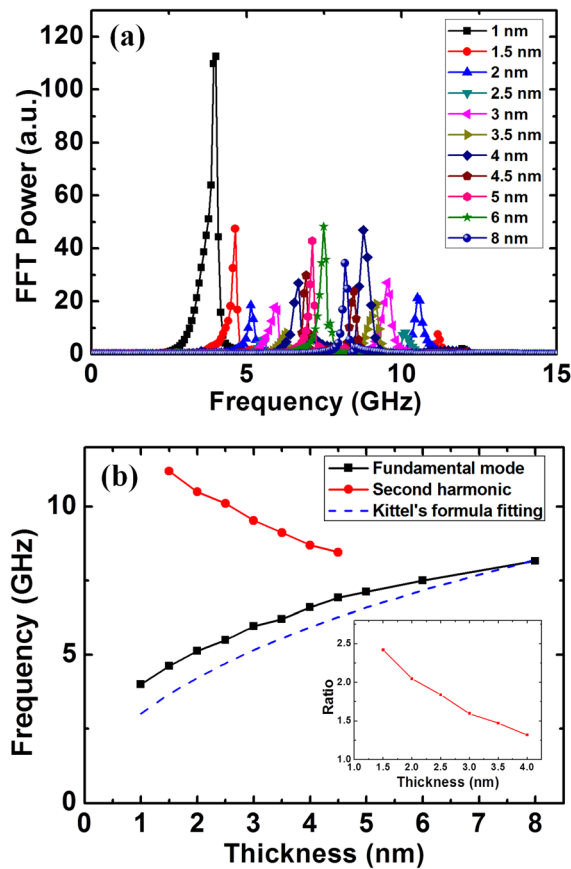
FIG. 4. (a) Power spectra for different thicknesses of the nanowire. (b) The frequency of the fundamental and the second harmonic modes as function of the nanowire thickness. Inset figure shows the ratio between the fundamental and second harmonic mode frequencies as a function of thickness of the nanowire.

thickness is varied from 1 nm to 8 nm. The frequency of the fundamental mode has shown a red shift as the thickness of the nanowire is decreased, which matches well with the Kittel's equation. More importantly, the result shows that the generated spin wave exhibits a second harmonic mode when the nanowire thickness is reduced below 5 nm. At a thickness of 4.5 nm, a second harmonic mode at $f = 8.5$ GHz is observed, which is approximately 1.2 times the frequency of the fundamental mode. The frequency of the second harmonic increases steadily as the thickness of the nanowire is decreased. For nanowire with $Ni_{80}Fe_{20}$ film thickness of 1.5 nm, the frequency of the second harmonic increases to 10.2 GHz. The presence of the second harmonic and its dependence on the nanowire thickness cannot be explained by using the Kittel's equation. As the $Ni_{80}Fe_{20}$ film thickness is reduced, the ratio of the frequency of the fundamental mode to the second harmonic mode increases, as seen in the inset of Fig. 4(b). This is analogous to the ratio between the fundamental and the second harmonic mode of the one-dimensional infinite quantum well.[28] This result suggests that for thin nanowire, the transverse spin wave can be thought to process mainly in the xy plane due to the shape anisotropy of the nanowire.

To understand better how the spin waves are affected by the in-plane applied field (H_a), the power spectra of a NW with width 100 nm and film thickness 6 nm as a function of different field strength are shown in Fig. 5. As the geometrical parameters are the same for all the simulations, the non-propagating mode displays a fixed frequency. With the increase of the field strength from 0.1 mT to 1 mT, the amplitude of the SW mode is increased. This can be explained by the increase in DW speed as the external field increases. The higher energy, the DW possesses, the more energy that needs to be dissipated during the collision process, resulting in higher amplitude of the fundamental mode.
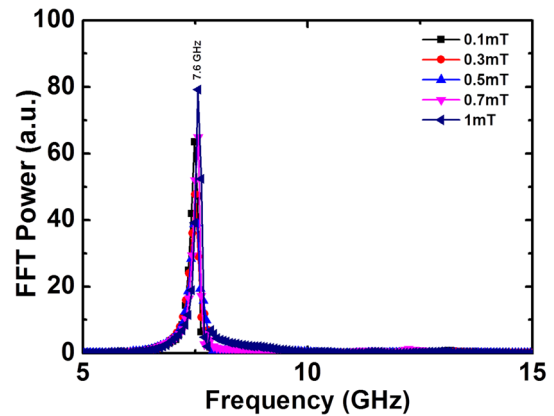
IV. CONCLUSION

In conclusion, we have investigated the characteristics of spin waves that are generated from the annihilation of two transverse DWs in a single nanowire. The frequency of the non-propagating mode of the spin wave is found to be independent of the applied field; instead, it is highly dependent of the nanowire dimensions. In general, the frequency of the generated spin wave decreases as the width of the nanowire is increased or its thickness is decreased. However, for nanowire with film thicknesses less than 5 nm, a second harmonic mode with a higher frequency appears. The appearance of the second harmonic modes can be attributed to the strong confinement along the z axis, which allows the magnetization to process in the xy plane. From application viewpoint, the nanowire should be engineered so that the resulting spin waves from the DW-DW collision do not affect the subsequent DWs next to it. The decay coefficient of the spin wave power suggests that the DWs in the memory device should be at least 300 nm apart for them to be free of interference from the spin waves. It also suggests that the thickness of the nanowire should not be reduced beyond 5 nm so that the second harmonic mode is not activated, as it is the high frequency spin wave that is detrimental to the dynamics of adjacent DWs.[10]

[1] D. A. Allwood, G. Xiong, C. C. Faulkner, D. Atkinson, D. Petit, and R. P. Cowburn Science **309**, 1688 (2005).

[2] M. Hayashi, L. Thomas, R. Moriya, C. Rettner, and S. S. P. Parkin, Science **320**, 209 (2008).

[3] S. S. P. Parkin, M. Hayashi, and L. Thomas, Science **320**, 190 (2008).

[4] J. A. Katine and E. E. Fullerton, J. Magn. Mater. **320**, 1217 (2008).

[5] J. Slonczewski, J. Magn. Magn. Mater. **159**, L1 (1996).

[6] L. Berger, J. Appl. Phys. **71**, 2721 (1992).

[7] L. Berger, Phys. Rev. B **54**, 9353 (1996).

[8] G. Tatara and H. Kohno, Phys. Rev. Lett. **92**, 086601 (2004).

[9] X. S. Wang, P. Yan, Y. H. Shen, G. E. W. Bauer, and X. R. Wang, Phys. Rev. Lett. **109**, 167209 (2012).

[10] M. Jamali, H. Yang, and K. J. Lee, Appl. Phys. Lett. **96**, 242501 (2010).

[11] S. Choi, K. S. Lee, K. Y. Guslienko, and S. K. Kim, Phys. Rev. Lett. **98**, 087205 (2007).

[12] Y. Au, M. Dvornik, O. Dmytriiev, and V. V. Kruglyak, Appl. Phys. Lett. **100**, 172408 (2012).

[13] R. Hertel and C. M. Schneider, Phys. Rev. Lett. **97**, 177202 (2006).

[14] A. Kunz, Appl. Phys. Lett. **94**, 132502 (2009).

[15] D. Djuhana, H. G. Piao, S. C. Yu, S. K. Oh, and D. H. Kim, J. Appl. Phys. **106**, 103926 (2009).

[16] A. Janutka, Phys. Rev. E **83**, 056607 (2011).

[17] M. J. Donahue and D. G. Porter, *OOMMF User's Guide, Version 1.0*, Interagency Report NISTIR 6376 (National Institute of Standards and Technology, Gaithersburg, MD, 1999).

[18] I. Purnama, M. Chandra Sekhar, S. Goolaup, and W. S. Lew, Appl. Phys. Lett. **99**, 152501 (2011).

[19] T. L. Gilber, IEEE Trans. Magn. **40**, 3443 (2004).

[20] D. Kumar, O. Dmytriiev, S. Ponraj, and A. Barman, J. Phys. D: Appl. Phys. **44**, 235002 (2011).

[21] A. Lara, V. Metlushko, and F. G. Aliev, J. Appl. Phys. **114**, 213905 (2013).

[22] B. Hillebrands and K. Ounadjela, *Spin Dynamics in Confined Magnetic Structure I* (Springer-Verlag, Heidelberg, Germany, 2002), pp. 65–89.

[23] K. Y. Guslienko, R. W. Chantrell, and A. N. Slavin, Phys. Rev. B **68**, 024422 (2003).

[24] B. A. Kalinikos and A. N. Slavin, J. Phys. C **19**, 7013 (1986).

[25] R. D. McMichael and M. J. Donahue, IEEE Trans. Magn. **33**(5), 4167 (1997).

[26] C. Kittel, Phys. Rev. **73**, 155 (1948).

[27] J. B. Yoon, C. Y. You, Y. H. Jo, S. Y. Park, and M. H. Jung, J. Korean Mag. Soc. **20**, 1 (2010).

[28] N. Zettili, *Quantum Mechanics Concepts and Applications* (Wiley, Chippenham, Wiltshire, 2009), pp. 215–248.